speaking honorarium from Abbott Vascular, Biotronik, Medtronic, and St. Jude Medical. Dr. Virmani receives research support from Abbott Vascular, Bio-Sensors International, Biotronik, Boston Scientific, Medtronic, MicroPort Medical, OrbusNeich Medical, SINO Medical Technology, and Terumo Corporation; has speaking engagements with Merck; receives honoraria from Abbott Vascular, Boston Scientific, Lutonix, Medtronic, and Terumo Corporation; and consults for 480 Biomedical, Abbott Vascular, Medtronic, and W. L. Gore. All other authors have reported that they have no relationships relevant to the contents of this paper to disclose.

REFERENCES

1. Burke AP, Farb A, Malcom GT, Liang Y, Smialek J, Virmani R. Effect of risk factors on the mechanism of acute thrombosis and sudden coronary death in women. Circulation 1998;97:2110–6.

2. Kolodgie FD, Burke AP, Farb A, et al. Differential accumulation of proteoglycans and hyaluronan in culprit lesions: insights into plaque erosion. Arterioscler Thromb Vasc Biol 2002;22:1642–8.

3. Ozaki Y, Okumura M, Ismail TF, et al. Coronary CT angiographic characteristics of culprit lesions in acute coronary syndromes not related to plaque rupture as defined by optical coherence tomography and angioscopy. Eur Heart J 2011;32:2814–23.

4. Jia H, Abtahian F, Aguirre AD, et al. In vivo diagnosis of plaque erosion and calcified nodule in patients with acute coronary syndrome by intravascular optical coherence tomography. J Am Coll Cardiol 2013;62:1748–58.

5. Prati F, Uemura S, Souteyrand G, et al. OCT-based diagnosis and management of STEMI associated with intact fibrous cap. J Am Coll Cardiol Img 2013;6:283–7.

Flare Spots in Intravascular Optical Coherence Tomography Images of Bioabsorbable Stents

Flare spots (Figures 1A and 1B) are observed in intravascular optical coherence tomography (IVOCT) images of bioabsorbable stent struts in patients and have no analog in metallic stents. Gutiérrez-Chico et al. (1) proposed that flare spots were located at hinge points where the highest strain is experienced during deployment, suggesting that they represent micro-crazes (fine lines) in the polymer. Nonetheless, the mechanism for the presence of flare spots in IVOCT images, and the large variation in their appearance where no two are alike, is not known. In this study, micro-CT and IVOCT images of a bioabsorbable stent deployed in a cylindrical phantom blood vessel were coregistered and compared in order to investigate the underlying mechanism for presence of flare spots in IVOCT images.

A 3-mm lumen diameter phantom vessel was made out of polydimethylsiloxane with elastic properties comparable to that of arteries. Titanium dioxide was added to polydimethylsiloxane to simulate the light-scattering properties of the arterial wall. A 3.0 $\times$ 18 Absorb stent (Abbott Vascular, Santa Clara, California) was deployed within the phantom vessel at 16-atm pressure with a balloon while submerged in a water bath at body temperature (37°C) to minimize any structural changes to the polymer. IVOCT images of the Absorb stent (Figures 1C and 1D) were acquired using a frequency domain IVOCT system (CorVue, Volcano Corporation, San Diego, California) while the phantom vessel was flushed with saline. The IVOCT catheter was pulled back at a slow speed of 1.5 mm/s over a 15-mm length of vessel recording at a rate of 30 frames/s. After stent deployment and IVOCT imaging, micro-CT images of the phantom vessel at resolution of 6 μm were recorded as a gold image standard. Each recorded IVOCT image was registered to a sequence of 8 micro-CT images due to the spiral pattern associated with a pullback and relatively larger longitudinal spacing between IVOCT images. Figure 1 illustrates 2 successive IVOCT images (Figures 1C and 1D) along with the corresponding coregistered micro-CT images (Figures 1E and 1F). The change in appearance of groups of struts (indicated with green and yellow ovals) can be observed in successive IVOCT and micro-CT images. From the micro-CT image sequence (Figures 1E and 1F), adjacent struts are observed to merge (separate) at the arterial side of the stent and form a micro-sized gap at the vessel wall, with a different appearance at every gap. Flare spots in the IVOCT images are only generated when gaps appear in the micro-CT images on the arterial side.

The micro-CT dataset was used to create a 3-dimensional representation of the entire stent demonstrating that micro-crazes are formed on the arterial side of the stent and therefore result in micro-gaps at the vessel wall. There were 2 types of crazing, which correspond to locations where 2 or 3 struts merge (separate). During a pullback, the IVOCT beam propagates through the vessel lumen, where portions of light reflect from and transmit across the strut edge. Light reflected from the strut edge forms an outline of the outer surface of the strut in IVOCT images. When the IVOCT beam enters a gap region with micro-crazes, reflections at the gap boundary occur before light returns to the catheter. The reflections at gap boundaries produce flare spots of higher intensity inside struts in IVOCT images (Figure 1G). Because each crazing site is different at every hinge point, as demonstrated by the micro-CT images (Figures 1E and 1F), the pattern of light reflections is expected to vary, which is consistent with the observation that no two flare spots appear identical in recorded IVOCT images.

In conclusion, we have completed imaging experiments of an Absorb stent deployed in a phantom vessel to investigate the origin of flare spots observed in IVOCT images of bioabsorbable stents. Flare spots observed in IVOCT images correspond to gaps observed in micro-CT images formed by micro-crazes

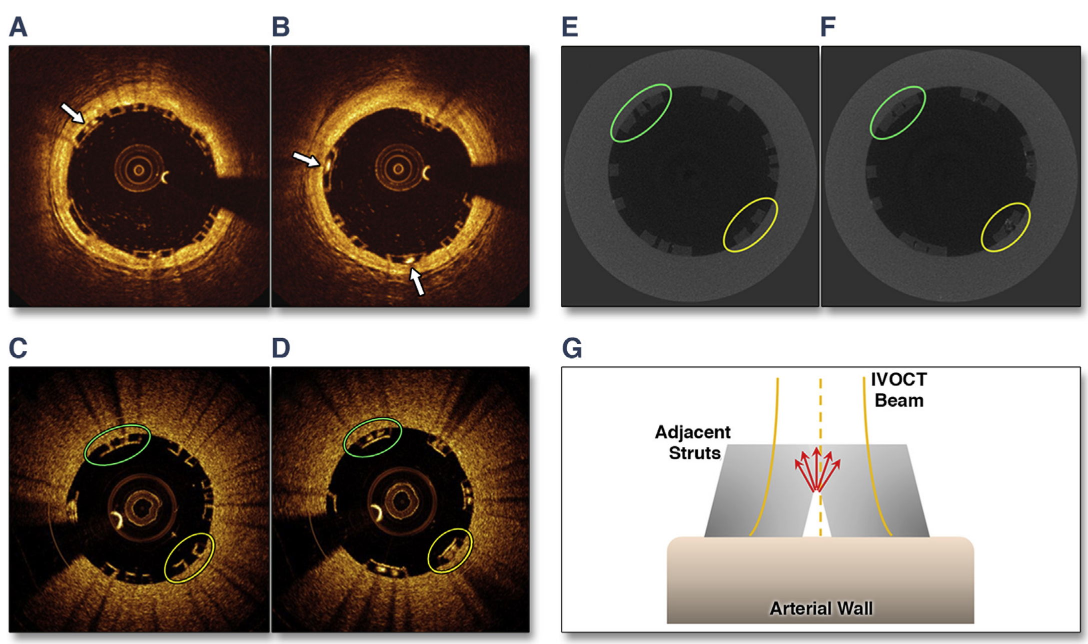

FIGURE 1 Flare Spots Observed in IVOCT Images of Absorb Stent

(A,B) Stent deployed in a patient coronary artery **(arrows); (C,D)** phantom vessel with successive intravascular optical coherence tomography (IVOCT) images at 100-μm intervals; and **(E,F)** corresponding micro-CT images at 50-μm intervals. Adjacent struts (**green and yellow ovals**) merge at the luminal side of the stents and form a gap at the vessel wall. **(G)** Reflections at gap boundaries result in flare spots.

on the arterial side of the stent. The appearance of flare spots in IVOCT images is consistent with light reflecting from surfaces formed at these gap boundaries before returning to the catheter.

Sahar Elahi, PhD
Thomas E. Milner, PhD
Richard J. Rapoza, PhD
Jouke Dijkstra, PhD
Marc D. Feldman, MD*
*University of Texas Health Science Center
Cardiac Catheterization Laboratory
Room 5.642 U
7703 Floyd Curl Drive
San Antonio, Texas 78229
E-mail: feldmanm@uthscsa.edu

http://dx.doi.org/10.1016/j.jcmg.2014.04.023

Please note: Dr. Rapoza is a full-time employee of and has equity in Abbott Vascular. All other authors have reported that they have no relationships relevant to the contents of this paper to disclose.

REFERENCE

1. Gutiérrez-Chico JL, Radu MD, Diletti R, et al. Spatial distribution and temporal evolution of scattering centers by optical coherence tomography in the poly(L-lactide) backbone of a bioresorbable vascular scaffold. Circ J 2012;76:342–50.

Cardiac Steatosis and Left Ventricular Dysfunction in HIV-Infected Patients Treated With Highly Active Antiretroviral Therapy

Heart disease is a major contributor to morbidity and mortality in persons infected with human immunodeficiency virus (HIV), and both HIV and highly active antiretroviral therapy (HAART) may be associated with abnormalities in cardiac function and metabolism (1). Ectopic fat deposition in cardiomyocytes constitutes one possible mechanism, especially considering the influence of HIV itself and HAART on the human metabolic milieu. To test this hypothesis, we studied 27 HIV-seropositive (+) cases on stable HAART (≥3 years) and 22 HIV-negative control subjects; neither group had history of personal or family history of cardiovascular disease.

Myocardial triglyceride content was measured by magnetic resonance spectroscopy (3T MAGNETOM Verio, Siemens, Germany) (2) and revealed a 3-fold elevation in cases compared with control subjects (**Figure 1A**). To assess left ventricular (LV) function, magnetic resonance tissue tagging was performed on a mid-ventricular short-axis image (3). Both peak